



**HAL**  
open science

## Multiscale NMR analysis of the degradation of apple structure due to thermal treatment

Alexandre Leca, Sylvie Clerjon, J.-M. Bonny, Catherine M. G. C. Renard,  
Amidou Traoré

### ► To cite this version:

Alexandre Leca, Sylvie Clerjon, J.-M. Bonny, Catherine M. G. C. Renard, Amidou Traoré. Multiscale NMR analysis of the degradation of apple structure due to thermal treatment. *Journal of Food Engineering*, 2021, 294, pp.110413. 10.1016/j.jfoodeng.2020.110413 . hal-03040113

**HAL Id: hal-03040113**

**<https://hal.inrae.fr/hal-03040113v1>**

Submitted on 15 Dec 2022

**HAL** is a multi-disciplinary open access archive for the deposit and dissemination of scientific research documents, whether they are published or not. The documents may come from teaching and research institutions in France or abroad, or from public or private research centers.

L'archive ouverte pluridisciplinaire **HAL**, est destinée au dépôt et à la diffusion de documents scientifiques de niveau recherche, publiés ou non, émanant des établissements d'enseignement et de recherche français ou étrangers, des laboratoires publics ou privés.



Distributed under a Creative Commons Attribution - NonCommercial 4.0 International License

1 Multiscale NMR analysis of the degradation of apple structure due  
2 to thermal treatment

3 Alexandre Leca<sup>\*a</sup>, Sylvie Clerjon<sup>b</sup>, Jean-Marie Bonny<sup>b</sup>, Catherine M.G.C. Renard<sup>c</sup>,  
4 Amidou Traore<sup>b</sup>

5 <sup>a</sup> INRAE, Avignon Université, UMR408 SQPOV, 84914 Avignon, France

6 <sup>b</sup> INRAE, AgroResonance, 63122 Saint Genès Champanelle, France.

7 <sup>c</sup> INRAE, TRANSFORM, 44316 Nantes, France

8 *\* Corresponding author: alexandre.leca@inrae.fr*

9

## 10 **Abstract**

11 The cooking temperature required to alter the structure of apple sticks was investigated  
12 by NMR (magnetic resonance imaging (MRI) and magnetic resonance spectroscopy  
13 (MRS)) to detect the thermal degradation of the vacuolar membrane, and by puncture  
14 tests to detect tissue softening due to heating. Both NMR methods evidenced the pivot  
15 temperature of 53 °C at which the apple parenchyma switches from “fresh” to “cooked”  
16 state, i.e. loses its cellular and subcellular structuration. At the tissue scale, the puncture  
17 tests performed on apple sticks also showed a shift in firmness at 53 °C. At the  
18 molecular scale, the NMR measurements converged with both MRI and MRS,  
19 evidencing a thermal degradation of the cell membranes leading to a change in vacuole  
20 water chemical exchanges and distribution throughout the cells, cell walls and  
21 intercellular spaces. These phenomena lead to a tissue homogenization with heating,  
22 which is reflected by a single  $T_2$  after cooking.

23

## 24 **Keywords**

25 NMR; relaxometry; puncture; thermal softening; apple; heat processing

26

## 27 **1. Introduction**

28

29 Understanding the response of fruit and vegetable microstructure to thermal treatment  
30 is the key to assess the bioavailability of their nutrients (Parada and Aguilera, 2007), as  
31 well as the texture of the fresh or processed product (Aguilera, 2005). However, because  
32 of the complexity of the products involved and their multiscale properties and  
33 microstructure, this relation between thermal treatment and fruit and vegetable

34 microstructure is still not completely understood. Two main mechanisms have long  
35 been identified, namely loss of cellular compartmentation and cell wall degradation, the  
36 later having been much more studied. However, during cooking, the first irreversible  
37 reaction is the disruption of vacuolar membrane, causing a loss of cellular turgor  
38 pressure and diffusion of vacuolar water (Waldron et al., 2003), which leads to a  
39 softened and less structured fruit.

40 Apple is a relevant model for this study because its intrinsic microstructure and cell  
41 organization have been extensively studied and are well documented (Janssen et al.,  
42 2020; Khan and Vincent, 1990): apple parenchyma is structured by a network of cell  
43 walls enclosing cells, mostly composed of water-rich vacuoles, and a high proportion of  
44 gas-filled intercellular spaces, almost 30% of the volume in mature apples (Chiralt and  
45 Fito, 2003; Mendoza et al., 2007). Most published works on apple texture concern  
46 maturing and stored fresh fruits, specifically showing the impact of the cell organization  
47 of apple parenchyma on the firmness and crunchiness of the fruits (Harker et al., 1997;  
48 Létal et al., 2003). The porosity, *i.e.* the ratio of intercellular air space to total volume,  
49 and the size of individual intercellular spaces, have been reported to contribute to apple  
50 firmness and crunchiness (Harker et al., 1997; Ting et al., 2013). The impact of the  
51 thermal treatment on fruit texture and quality is generally assessed through firmness  
52 analysis and physicochemical analyses (de Belie et al., 2002). However, only a few  
53 studies have looked at the relationship between mechanical properties and the evolution  
54 of cellular structure (Kebe et al., 2015; Ng and Waldron, 1997). An efficient analytical  
55 technique for monitoring microstructural changes is therefore needed.

56 Nuclear magnetic resonance (NMR) and its two modalities, nuclear magnetic resonance  
57 spectroscopy (MRS) and imaging (MRI), are non-destructive and will detect objects that  
58 are not modified by sample preparation. They allow to visualize and quantify the  
59 heterogeneity in plant materials such as apple flesh (Winisdorffer et al., 2015), and to  
60 study the evolution of fruits during storage at a high spatial resolution, revealing  
61 otherwise undetectable variations (Ciampa et al., 2010).

62 More specifically, MRS is a method of choice to measure fine tissue interactions with  
63 water through the proton relaxation time interaction at the sample scale, and non-  
64 destructively. Gonzalez et al. (Gonzalez et al., 2010) used it on onions to study the  
65 decrease in transverse relaxation time of the main water fraction with increasing  
66 cooking temperature, and showed the destruction of cellular structure leading to an  
67 increased exchange between water and cellular content. The evolution of the subcellular  
68 structure of apple parenchyma in drying or freezing processes clearly shows that  
69 changes to cell wall and cell membrane impact the transverse relaxation time (Hills and  
70 Remigereau, 1997). The membranes, which are still intact, act as a barrier against water  
71 exchange, and result in **a multicomponent  $T_2$  distribution**.

72 MRI is well suited to locally quantify water concentration or how water bonds to the  
73 other constituents, but at a finer spatial scale. Already in 1991, McCarthy et al  
74 (McCarthy et al., 1991) followed the water content in drying apple slices using MRI. The  
75 indirect measurement of  $T_2$  and  $T_2^*$  maps, which are sensitive to discrepancies in  
76 magnetic susceptibility, is used to describe the microstructure of plant tissues, while  
77 preserving the sample integrity, and thus enables longitudinal study. **NMR relaxometry**  
78 **methods combining MRI and MRS lets quantify (i) the relaxation time and water**

79 compartmentalization in tissues, (ii) the  $T_2$  and permeability of cell membranes, and  
80 (iii) the diffusion and magnitude of cell and intercellular transport (Van As, 2007).

81 MRI is thus a relevant approach for studying vacuolar membrane thermal degradation  
82 and the subsequent diffusion of intracellular fluid filling the intercellular spaces during  
83 and after thermal treatment. This method is mainly limited by its time resolution:  
84 several minutes are required to produce images or spectra yielding specific parameters  
85 describing the spatial distribution and mobility of water molecules, *i.e.* relaxation time  
86 and diffusion coefficients. Acquisition time may be shortened either by decreasing the  
87 image spatial resolution, *e.g.* as in the study of Mohoric on rice (Mohoric et al., 2009),  
88 or by optimizing k-space filling, as in the study of meat cooking by Bouhrara et al.  
89 (Bouhrara et al., 2012). However, existing studies focus on fresh fruits (Marigheto et al.,  
90 2008; Van As and van Duynhoven, 2013) or on fruit-based model materials to  
91 reproduce cellular degradation (Lahaye et al., 2018), and not on intrinsically structured  
92 processed products.

93 This study addresses the hypothesis that the apple tissue thermal softening occurs as a  
94 consequence of or simultaneously with the thermal degradation of the vacuolar  
95 membrane, changing the tissue microstructure. To our knowledge, no study has  
96 investigated the critical temperature at which the cell membranes of a fruit is highly  
97 damaged. **NMR relaxometry (both imaging and spectroscopy)** was used to objectify the  
98 membrane fusion temperature in the apple parenchyma on a non-processed whole fruit  
99 sample. For this purpose, apple fruit samples were treated at different temperatures  
100 (below and above tissular destructuration) prior to characterization by penetrometry,  
101 **and NMR relaxometry. MRS relaxometry resolves multiple  $T_2$  compartments in the**

102 whole sample, while MRI is sensitive to microstructural heterogeneities at a finer spatial  
103 scale.

## 104 **2. Materials and methods**

### 105 2.1 Plant material

106 Golden Delicious apples (*Malus domestica* Borkh. var. Golden Delicious) were  
107 purchased at a local supermarket (Auchan, Avignon, France) at consumable ripeness.  
108 They were stored in a cold chamber at +4 °C in normal atmospheric conditions for less  
109 than 8 days, and were taken out approximately 4 hours before the experiment for  
110 equilibration at room temperature. For each condition, apples were cut into 12 × 8 × 30  
111 mm<sup>3</sup> sticks, the longer side being cut along the radial axis of the apple. Sticks to be  
112 cooked were vacuum-sealed in food-grade plastic bags (PE-LD 30 µm, RAJA SA,  
113 Tremblay-en-France, France). For the NMR measurements, six apple sticks were used  
114 for each condition, each one from a different fruit. For the puncture tests, three sticks  
115 were cut from both sides of an apple, except for smaller apples in which only two sticks  
116 were sampled.

### 117 2.2 Thermal treatments

118 The thermal treatments were performed in a water bath, three apple sticks at a time.  
119 The times needed to reach each cooking temperature at the center of two sticks were  
120 measured in a preliminary study by inserting a thermocouple during heating; these  
121 times were then used for subsequent experiments at the corresponding temperatures.  
122 Consequently, the five thermal treatments were: 7 min at 45 °C, 10 min at 50 °C, 10 min  
123 at 53 °C, 14 min at 60 °C and as a reference for a complete thermal denaturation, 18 min  
124 at 70 °C. After thermal treatment, samples were cooled in melting ice for 8-15 minutes.

125 Samples were then kept at ambient temperature for 24 hours before measurement. This  
126 24 h rest before measurement was applied because a preliminary study (*data not*  
127 *shown*) had demonstrated a continuous evolution of the water status inside the apple  
128 sticks occurred for 6 hours following the treatment and cooling steps.

### 129 2.3 Firmness measurements

130 The firmness of the samples was estimated by measuring the mean load obtained from  
131 puncture tests, after preliminary tests (*data not shown*) had shown good repeatability at  
132 the apple stick scale. Each sample was punctured on two faces (one along the radial axis  
133 of the fruit, the other perpendicular to the radial axis), with two repetitions per face. The  
134 puncture tests were done using a Ta-Plus texturometer (Lloyd Instruments Ltd., Bognor  
135 Regis, UK) equipped with a 50 N load cell and a punch 2 mm in diameter and 17 mm  
136 long. Penetration rate was 100 mm.min<sup>-1</sup> and puncture stopped once a 70% strain was  
137 reached. Mean load at the plateau ( $F_{\text{mean}}$ , N) was determined for each test as the average  
138 of 1000 data points taken from the plateau region in the force-displacement curve.

### 139 2.4 NMR Relaxometry

140 **Both MRI and MRS relaxometry measurements** were made on a 9.4 T Bruker  
141 Ascend 400WB instrument (Bruker, Ettlingen, Germany) equipped with a  
142 microimaging accessory and using a 32 mm diameter birdcage radiofrequency coil used  
143 for both excitation and signal reception, at 20 °C.

#### 144 2.4.1 MRI $T_2$ measurement:

145 Each of the 30 samples (raw, 45 °C, 50 °C, 53 °C and 60 °C × 6 repetitions) was placed  
146 in a 25 mm tube with a reference stick (cooked for 18 min at 70 °C). Nine transversal



147 single spin echo images were acquired, intercepting both the reference and the cooked  
148 sample, at nine different echo times (6.5, 8.5, 10.5, 15, 20, 40, 70, 100 and 200 ms), TR  
149 = 3000 ms, voxel vol. 1 mm<sup>3</sup> isotropic, total acquisition time 32 min. The  $T_2$  maps were  
150 built by fitting these nine echo magnitudes voxelwise, assuming mono-exponential  
151 decrease. **The  $T_2$  histogram was calculated over the six sample images, for the six**  
152 **durations and temperature conditions.**

153 **For morphological analysis, high resolution MRIs were acquired in the same**  
154 **experimental conditions: transversal multi-slice mono-echo image; TE/TR = 5.5/3000,**  
155 **spatial resolution 0.1 × 0.1 × 0.5 mm<sup>3</sup>, field of view 1.6 × 3 cm, acquisition time 32**  
156 **minutes.**

#### 157 2.4.2 MRS $T_2$ measurement:

158 Spectroscopic  $T_2$  measurements were performed using the Carr-Purcell-Meiboom-Gill  
159 (CPMG) pulse sequence,  $90_x^\circ - \tau - [180_y^\circ - \tau - (\text{echo})]_n$ , with an interpulse delay  $\tau$  of 500  $\mu\text{s}$ .  
160 This relatively short sampling time was used to minimize diffusion dephasing while  
161 being large enough to avoid sample overheating by RF deposition. The recycle delay  
162 (time to let the signal recover between successive echo acquisitions) was set to 2 s. A  
163 total of  $n = 256$  echoes spectra were recorded to describe the transversal echo decay  
164 curve for a total acquisition time of 45 min. For each time/temperature treatment (**same**  
165 **as in imaging measurements, except that the sample cooked at 70°C was measured**  
166 **separately**),  $T_2$  measurements were performed on six samples to improve robustness.

167 A common feature in biological systems is a continuous distribution of water among  
168 their internal structures (Kroeker and Henkelman, 1986). Continuous water dynamic  
169 distribution will therefore better reflect the biological microstructure of the apple

170 parenchyma. To estimate such continuous distribution, the measured  $T_2$  decay curves  
171 were fitted by a weighted sum of a large number  $m$  of exponentials:

$$172 \quad \mathbf{S} = \sum_{j=1}^m A_j e^{\left(-t_i/T_{2j}\right)} \quad i = 1, 2, \dots, n \quad [1]$$

173

174 Each fitting was performed with an in-house Matlab® implementation of the non-  
175 negative least squares (NNLS) algorithm (Lawson and Hanson, 1995). The solution  
176 given by NNLS is a sparse vector of  $m$  discrete  $A_j$  non-zero amplitudes at known  $T_{2j}$   
177 values of the given basis (Whittall and MacKay, 1989). A standard regularization  
178 constraint was added to smooth the estimated discrete distribution  $A_j$  provided by  
179 NNLS. The resulting distributions of  $T_2$  relaxation times do not require defining the  
180 number of exponentials beforehand, only to feed the regularized NNLS algorithm with a  
181 large number of  $T_{2j}$  values (*i.e.* 200) logarithmically spaced from 1 ms to 1000 ms. The  
182 regularized NNLS solution was a set of amplitudes  $A_j$  that minimizes the lack of fit:

$$183 \quad \sum_{i=1}^N \left| \sum_{j=1}^M A_{ij} S_j - y_i \right|^2 + \mu \sum_{j=1}^M |S(T_{2j})|^2, \mu \geq 0 \quad [2]$$

184 where the Lagrangian term  $\mu$  is automatically calculated using the cross validation  
185 approach (Whittall and MacKay, 1989).

186 To ease comparison with  $T_2$  maps from imaging measurements, a weighted average of  
187 all  $T_2$  components was also calculated.

188

### 189 **3. Results**

#### 190 3.1 Texture analysis

191  $F_{\text{mean}}$  decreased as the heating temperature increased (Figure 1), in agreement with the  
192 authors' visual and tactile observations, and the thermal softening of fruits and  
193 vegetables observed in previous studies (Bourles et al., 2009; Ng and Waldron, 1997).  
194 Although the value dispersion was high, especially for the apple sticks heated at 53 °C,  
195 significant differences were found between three groups: {raw, 45°C, 50°C}, {53°C}, and  
196 {60 °C, 70 °C}.

197 The average value of  $F_{\text{mean}}$  at 53 °C is equal to 1.16 N, which is almost halfway between  
198  $F_{\text{mean}}$  at 50 °C (1.75 N) and at 60 °C (0.5 N).

199

### 200 3.2 Imaging and Spectroscopy Relaxometry analyses

201 Figure 2 presents the  $T_2$  maps obtained on six samples per temperature and duration  
202 condition. Because local  $T_2$  never exceeded 60 ms,  $T_2$  maps were windowed from 0 to 60  
203 ms. On each image, samples cooked for 18 min at 70 °C (reference final thermal  
204 degradation) are presented on the left, and samples obtained with the indicated  
205 treatment temperature and duration on the right.

206 **MRI relaxometry:** The distributions of  $T_2$  within the samples calculated for each thermal  
207 treatment from MRI  $T_2$  maps are displayed in the middle part of Figure 2. For the raw  
208 samples,  $T_2$  values were very short and closely distributed around 9 ms. When the  
209 treatment temperature increased, higher  $T_2$  values appeared, mainly between 30 and 50  
210 ms. For 70 °C,  $T_2$  maps of all the reference samples (on the left in each photo in Figure  
211 2) were used to obtain the  $T_2$  distribution.

212 **MRS relaxometry:** The distribution of water proton  $T_2$  displayed three components for  
213 the six raw samples with the relative amplitudes of 70–80% for the largest  $T_2$   
214 component, 20–30% for the intermediate one and 1–5% for the lowest peak amplitude.

215 The positions of the  $T_2$  peaks were variable, which can be attributed to the intrinsic  
216 signal-to-noise ratio of the decay curve of each sample (see supplementary data, Figure  
217 S3). However, considering the apple cellular structure and its compartmentalization  
218 (Hills and Remigereau, 1997), the largest  $T_2$  component (20–60 ms) can be attributed to  
219 the water in vacuoles. The intermediate peak, with a  $T_2$  value of around 100 ms, can be  
220 assigned to water in cytoplasm, and the population with the shortest relaxation times  
221 (around 10 ms) may be attributed to water in tight interactions with membranes and/or  
222 macromolecules. The observation of three distinct relaxation times implied that the  
223 diffusive exchanges between the different apple compartments were slow compared to  
224 the sampling time, i.e., echo time (Belton and Ratcliffe, 1985). However, the observed  $T_2$   
225 values differed slightly from those already reported from low-field studies (Hills and  
226 Remigereau, 1997). For the  $T_2$  distribution obtained with CPMG (Figure 2, right), apple  
227 heating caused a separation into two main populations (around 25 ms and 220 ms).  
228 Indeed, the marked difference shown by samples subjected to 45 °C was the  
229 disappearance of the lowest  $T_2$  component. After treatment at 50 °C, samples still  
230 displayed two main  $T_2$  peaks, but the difference between their respective relaxation  
231 times was small. The samples treated at 53 °C showed a distinctive pattern, with a sharp  
232 separation between the  $T_2$  pools and a marked decrease in the  $T_2$  values (~30 ms) of the  
233 largest component. After cooking at 60 °C, the two components were clearly separated,  
234 with a marked decrease in the lowest component, which was shifted toward the longest  
235  $T_2$  (100–500 ms). The sample subjected to the cooking temperature of 70 °C (the  
236 reference sample) displayed one dominant component (>95%) with  $T_2 = 30$  ms.  
237 Thermal treatment resulted first in the reduction of the number of  $T_2$  components (from  
238 3 to 2) at lower temperature with a sharp separation observed at 53 °C. Further increase

239 in temperature led to the appearance of one dominant peak (> 95%) with a slight  
240 decrease in  $T_2$ .

241 Figure 3 shows, on the same graph, the evolution of both imaging  $T_2$  and weighted  
242 average non-resolved  $T_2$  values versus the cooking temperature. For the fresh sample,  
243 the imaging  $T_2$  value was lower than the spatially non-resolved one, whereas these  
244 values converged to nearly the same value at temperatures above 53 °C.

245 Figure 4 presents high-resolution images of raw, and 50, 53 and 60 °C treated samples.  
246 The left sticks are the reference cooked (70 °C) samples. Despite the high water content  
247 of apple parenchyma, MRI in Figure 4 showed a very poor signal on raw samples. Even  
248 at this high spatial resolution, the presence of air-filled spaces in non- or partially-  
249 cooked sample led to signal loss.

250

#### 251 **4. Discussion**

252 Contrast in MRI of biological systems relies on the interplay of various parameters, *e.g.*  
253 relaxation times, temperature, diffusion, flow and exchange, and on local differences in  
254 magnetic susceptibility (Belton and Ratcliffe, 1985). MRI acquisitions were designed to  
255 characterize the effect of treatment temperature on the apple parenchyma by means of  
256 the  $T_2$  relaxation maps. **The observed  $T_2$  maps from MRI and those from MRS CPMG  
257 results come from the interplay of various relaxation mechanisms (mainly, diffusive and  
258 chemical exchanges) related to the experimental conditions (mainly, echo time) and  
259 tissue characteristics (compartments size, membrane permeability, porosity, etc...). The  
260 contribution of each relaxation mechanism, among others, to the observed  $T_2$  have to be  
261 taken in account in the interpretation of the results of the present study. Indeed, to  
262 better explain the observed differences in  $T_2$  between imaging and spectroscopy and**

263 those between raw and cooked sample, the generic expression of the observed  $T_2$   
264 relaxation was used (Edzes et al., 1998):

$$265 \quad \frac{1}{T_{2obs}} = \frac{1}{T_{2i}} + \frac{1}{T_{2exc}} + \frac{1}{T_{2g}} \quad [3]$$

266 where  $T_{2i}$  represents the intrinsic water  $T_2$  in apple tissue,  $T_{2exc}$  represents the  
267 contribution of diffusive and/or chemical exchange effects seen in both imaging and  
268 spectroscopic experiments.  $T_{2g}$  comes from additional spin dephasing introduced by  
269 spatial encoding gradients in imaging experiments. The latter was negligible because  
270 one image acquisition per echo time was used instead of a multi-echo pulse sequence.

271 Air-filled spaces are known to account for 20 to almost 30% of the total volume of fresh  
272 apple parenchyma (Chiralt and Fito, 2003; Mendoza et al., 2007). Strong local magnetic  
273 field gradients ( $G_{loc}$ ) originate from the differences in magnetic susceptibility at the air-  
274 tissue and air-water interfaces. As a result, water diffusion through these local gradients  
275 leads to an increasing contribution of  $T_{2exc}$  and consequently in a reduction of the  
276 observed  $T_2$  value. The amount of this diffusive contribution is related to  $G_{loc}$  and echo  
277 time (TE) according to the expression:

$$278 \quad \frac{1}{T_{2exc}} \sim \gamma^2 G_{loc}^2 TE^2 D \quad [4]$$

279 where  $\gamma$  is the proton gyromagnetic ratio, and  $D$  is the diffusion coefficient of water in  
280 apple tissue. Equation [4] clearly explains the predominant effect of water diffusion  
281 through local field inhomogeneities on the lower signal intensity of spin echo images,  
282 and the resulting lower  $T_2$  values. Both the observed lower signal intensity in the  $T_2$   
283 weighted images of raw samples along with those cooked at temperature below  $53^\circ\text{C}$   
284 (Figure 4) and the lower  $T_2$  values from  $T_2$  maps of these samples (Figure 2) appear  
285 counterintuitive given the highly mobile water located in the apple parenchyma.

286 However, this phenomenon is commonly reported in fruits or plants (Van As, 2007).  
287 Even at the shortest imaging echo time (5 ms), water diffusion through apple  
288 compartments is the predominant  $T_2$  relaxation mechanism resulting also in the  
289 observed single averaged  $T_2$ , thus limiting the quantitative information about water  
290 compartmentalization along with changes related to the cooking process. Decreasing TE  
291 is one of the ways to minimize such diffusion effects on the measured  $T_2$  (Equation [4]).  
292 This can be achieved only with special MRI pulse sequences (Edzes et al., 1998) with  
293 some constraints outside the scope of the present study. One of the simple means, as  
294 used in the present study, to allow  $T_2$  measurements with short enough TE is by non-  
295 spatially resolved techniques. The CPMG measurement performed with the TE of 0.5 ms  
296 yielded a distribution of  $T_2$  relaxation time, which was in close agreement with water  
297 compartmentalization in apple tissue. The observation of multiexponential components  
298 also suggested that the diffusion between compartments (*i.e.* the  $T_{2exc}$  component in  
299 Equation [3]) is less efficient than in imaging. **The raw apple internal membranes**  
300 **(mainly the vacuolar membrane) act as a diffusion barrier (Belton and Ratcliffe, 1985)**  
301 **leading to the resolution of more than one exponential decays (components).** Equation  
302 [4] also indicates that the diffusion effect is mitigated at low field ( $G_{loc}^2$  depends on the  
303 field strength). This field dependency explains why our spectroscopic  $T_2$  values were  
304 smaller than those reported in the lower field studies by Hills and Duce (Hills and Duce,  
305 1990) and by Hills and Remigereau (Hills and Remigereau, 1997).  
306 **Figure 2 shows that the main result of increasing the cooking temperature was to**  
307 **increase, from the outer to the inner, the  $T_2$  values of the apple parenchyma, which**  
308 **became either nearly homogeneous for sample cooked at 53°C or fully homogeneous for**

309 those cooked at 60°C and 70°C. Similar behavior was observed for signal intensity of  
310 apple parenchyma in the high resolution T<sub>2</sub> weighted images (Figure 4). As stated  
311 above, the lower T<sub>2</sub> of the raw apple parenchyma (T<sub>2</sub> maps) along with its lower signal  
312 intensity in T<sub>2</sub> weighted images, regardless of high and mobile vacuolar water, are  
313 related to the large amounts of air-filled spaces in the apple tissue, i.e., the susceptibility  
314 effects. Consequently, the observed increase in the T<sub>2</sub> values in the cooked samples can  
315 reasonably be attributed to a decrease or the disappearance of these air-filled spaces.  
316 Furthermore, both imaging and spectroscopic T<sub>2</sub> results showed a marked change at  
317 treatment temperature 53 °C. Consequently, we chose to analyze the cooking effect on  
318 T<sub>2</sub> relaxation time for the two states, namely fresh *vs* cooked (before and after 53°C)  
319 rather than following T<sub>2</sub> components as a function of treatment temperature.

320 Between 45 °C and 50 °C, thermal treatment merely induced the disappearance of the  
321 low mobility water fraction, the one attributed to the water fraction in tight interaction  
322 with membranes and/or macromolecules. This disappearance may be ascribed to the  
323 shift toward lower relaxation time not resolved by the NNLS algorithm. This is  
324 anticipated by a lower signal-to-noise ratio (SNR) of these transversal decay signals. As  
325 demonstrated by Bertero and Pike (Bertero et al., 1982) and further discussed by  
326 Istratov and Vyvenko (Istratov and Vyvenko, 1999), SNR in the CPMG decay curve is a  
327 major factor that limits the resolution of exponential analysis. Figure 3 shows that after  
328 a 45 °C and even after a 50 °C thermal treatment, the difference between the imaging T<sub>2</sub>  
329 and the averaged spatially non-resolved T<sub>2</sub> remained unchanged in comparison with raw  
330 samples, indicating that diffusion was still dominant as the air-filled spaces were still  
331 dominant. This was confirmed by the high-resolution images (Figure 4). The presence of



332 these dominant air-filled spaces along with the presence of two main  $T_2$  components  
333 suggests that the integrity of the vacuolar membrane was still preserved at 40–50 °C.  
334 Beginning at 53 °C and more pronounced at 60 °C, high resolution images (Figure 4)  
335 and the  $T_2$  map (Figure 2, left) showed an increasing signal intensity in the apple  
336 parenchyma. As stated above, this increase in signal intensity was associated with the  
337 disappearance of the air-filled spaces, most probably owing to the internal membrane  
338 leakage. The latter hypothesis was supported by the appearance of one main  $T_2$   
339 component from the spatially non-resolved CPMG analysis. As no significant changes in  
340 volume of the apple sticks were observed (Figure 4), the disappearance of these air-filled  
341 spaces may be due to their filling with vacuolar water after membrane leakage.  
342 Goodman et al. (1996) have already reported this phenomenon in their study on  
343 strawberry fruit. They attributed the reduced inhomogeneity of the local magnetic  
344 susceptibility associated with the contamination of the parenchyma by *Botrytis cinerea*  
345 to filling of the intercellular gas spaces with intracellular fluid released through cell wall  
346 damages (Goodman et al., 1996). By 53 °C, the  $T_2$  values from imaging maps equaled the  
347 weighted average spatially non-resolved  $T_2$  (Figure 3). This convergence is predicted by  
348 Equation 4. The disappearance of air-filled spaces owing to cooking minimizes the  
349 contribution of diffusion through internal field gradients in the observed  $T_2$ . The latter  
350 becomes almost independent in TE used in imaging and spectroscopy CPMG (Figure 3).  
351 However, these  $T_2$  values (30–40 ms) remained smaller than those reported from lower  
352 field studies and with lower TE (Hills & Duce, 1990). These differences can this time be  
353 attributed to chemical exchanges between water protons and exchangeable protons  
354 belonging to macromolecules, *e.g.* polysaccharides. This phenomenon is well  
355 documented in the literature and the reader will find a characteristic description for the

356 apple in the work of Hills and Duce (Hills & Duce, 1990). In short, in the absence of  
357 diffusion within internal magnetic field susceptibility, at long TE, the additional  
358 dephasing due to chemical exchanges in the observed  $T_2$  (*i.e.*  $T_{2exc}$  in Equation [3])  
359 becomes effective and more pronounced at high magnetic field strengths with the  
360 increased difference in the chemical shifts between the exchangeable sites, namely water  
361 protons and protons belonging to macromolecular exchangeable sites.

362 The relevance of considering two states (uncooked under 53 °C and cooked from 53 °C)  
363 rather than each thermal treatment separately, as evidenced by the NMR study, is  
364 confirmed by the texture analysis, the  $F_{mean}$  results being divided into three groups :  
365 under 53 °C (uncooked), 53 °C (transitional temperature), above 53 °C (cooked).

366 This resistance to heat up to 50 °C is in line with previous findings (Kim et al., 1993). To  
367 our knowledge, no study has been performed on moderately high temperatures: existing  
368 studies are either at temperatures below 50°C or above 90 °C (Bourles et al., 2009), nor  
369 on the transitional temperature at which apple parenchyma softens.

370 However, existing studies focusing on fruit thermal treatment show the release of  
371 vacuolar water due to the thermal degradation of the vacuolar membrane and other  
372 cellular membranes as the first cause of apple tissue thermal degradation (Kunzek et al.,  
373 1999). This is followed by complex and non-comprehensively documented hydrolysis  
374 mechanisms occurring within the cell wall and inducing further thermal softening,  
375 especially at high temperatures (Christiaens et al., 2016; Van Buren, 1979), added to a  
376 potential degradation of the water sorption capacity of the cell wall during or after  
377 thermal treatment (Kebe et al., 2015; Le Bourvellec et al., 2011). **The endogenous**  
378 **enzymes, especially the pectin methylesterase (PME), can also modify the**  
379 **microstructure (Kunzek et al., 1999). Apple PME has low activity at the natural pH of**

380 apple (Denes et al., 2000) and it is stable in apple below 60 °C (El-Shamei et al., 2008),  
381 although once purified its activity rapidly decreases when heated above 52 °C (Denès et  
382 al., 2000). Endogeneous enzymes modify the cell wall resulting in two contrasted  
383 consequences: the joint action of PME and polygalacturonase leads to cell wall  
384 degradation (Sams et al., 1993), but the PME activity on its own may lead to consecutive  
385 demethylated galacturonic sequences that form gels with calcium and strengthen the  
386 cell walls (Barry-Ryan, 2012; Waldron et al., 2003). These enzymatic modifications of  
387 the cell wall could be increased by the thermal degradation of the vacuolar membrane,  
388 facilitating the access to cell wall for the PME.

389 The cooked apples sticks had a gel-like aspect, with a glassy appearance, whereas the  
390 uncooked sticks were opaque. This observation results of the air substitution with  
391 vacuolar water and is in agreement with spectroscopic studies on degraded fruit tissue  
392 (Valero et al., 2004; Zerbini et al., 2002). During sample preparation, cutting a raw stick  
393 produced qualitatively more juice than cutting a cooked stick. Such change would lead  
394 to the compartmentization and distribution of the cellular content within the whole  
395 tissue, at temperatures higher than or equal to 53 °C. This in turn results in a cloudiness  
396 and an enhanced fluid retention in the cell wall, expressed in the MRS results as a  
397 decreased  $T_2$ .

398

## 399 **5. Conclusion**

400 NMR  $T_2$  relaxometry was used to examine Golden Delicious apple fruit microstructure  
401 after thermal treatment. **Both MRI and MRS relaxometry** detected the thermal damage  
402 of cell membrane resulting in the leakage of vacuolar water and the filling of  
403 intercellular spaces, revealed by a clear shift in  $T_2$  patterns at the pivot temperature of

404 53 °C. The parallel firmness analysis evidenced to determine that the softening of apple  
405 parenchyma occurred simultaneously at 53 °C. Thus there was no detectable delay  
406 between the molecular and the tissue response of apple to thermal treatment, enabling a  
407 direct control of cooking and its impact on firmness and the chemical exchanges within  
408 the tissue. Although all *Malus domestica* cultivars have the same microstructural  
409 properties, differences in chemical composition of the vacuole, turgor pressure in cell,  
410 composition of the cell wall, are likely to impact the cell membrane resistance to thermal  
411 treatment, therefore the pivot temperature between raw and cooked. Thus this work  
412 only confirms 53 °C as the cooking temperature for Golden Delicious cultivar.  
413 This multiscale study also confirms that **NMR T<sub>2</sub> relaxometry** allows to explain the  
414 microstructural impact of thermal treatment, and to detect the transition temperature  
415 between raw and cooked, which correlates with texture loss.

416

### 417 **Acknowledgements**

418 All NMR experiments were performed at the AgroResonance Platform, INRAE (DOI  
419 10.15454/1.5572398324758228e12). This work was funded by INRAE TRANSFORM  
420 Research Department.

421

### 422 **CRedit authorship contribution statement**

423 **Alexandre Leca**: Conceptualization; Methodology; Investigation; Supervision; Writing  
424 – original draft. **Sylvie Clerjon**: Investigation; Methodology; Writing – original draft.

425 **Jean-Marie Bonny**: Supervision; Writing – review & editing. **Catherine MGC**

426 **Renard**: Supervision; Writing – review & editing. **Amidou Traore**: Investigation;

427 Methodology; Writing – original draft.

428 **References**

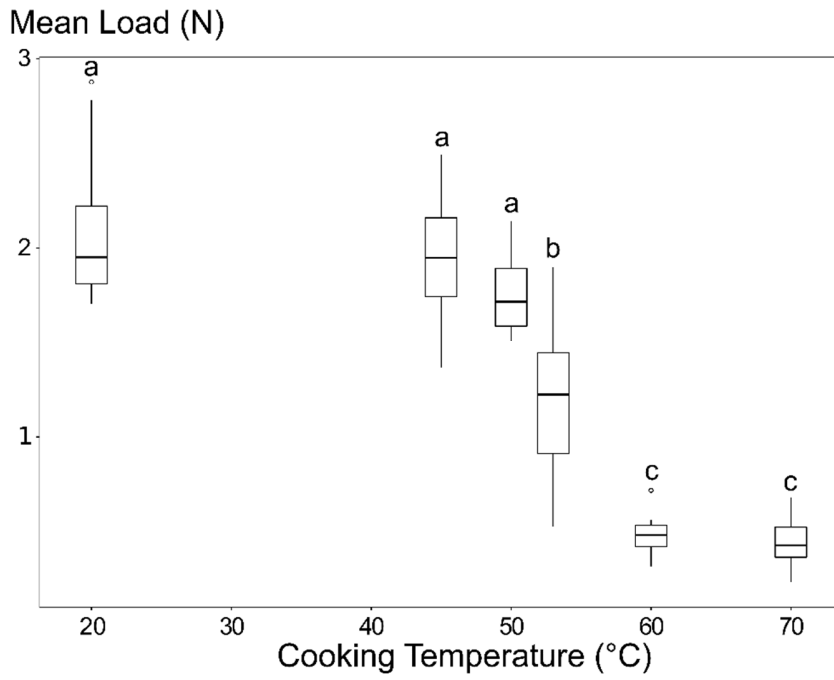
- 429 Aguilera, J.M., 2005. Why food microstructure? *Journal of Food Engineering* 67, 3–11.  
 430 <https://doi.org/10.1016/j.jfoodeng.2004.05.050>
- 431 Belton, P.S., Ratcliffe, R.G., 1985. NMR and compartmentation in biological tissues.  
 432 *Progress in Nuclear Magnetic Resonance Spectroscopy* 17, 241–279.  
 433 [https://doi.org/10.1016/0079-6565\(85\)80010-8](https://doi.org/10.1016/0079-6565(85)80010-8)
- 434 Bertero, M., Boccacci, P., Pike, E.R., 1982. On the recovery and resolution of exponential  
 435 relaxation rates from experimental data: a singular-value analysis of the Laplace  
 436 transform inversion in the presence of noise. *Proceedings of the Royal Society of*  
 437 *London. A. Mathematical and Physical Sciences* 383, 15–29.  
 438 <https://doi.org/10.1098/rspa.1982.0117>
- 439 Bouhrara, M., Clerjon, S., Damez, J.-L., Kondjoyan, A., Bonny, J.-M., 2012. In Situ  
 440 Imaging Highlights Local Structural Changes during Heating: The Case of Meat.  
 441 *J. Agric. Food Chem.* 60, 4678–4687. <https://doi.org/10.1021/jf2046569>
- 442 Bourles, E., Mehinagic, E., Courthaudon, J.L., Jourjon, F., 2009. Impact of vacuum  
 443 cooking process on the texture degradation of selected apple cultivars. *Journal of*  
 444 *Food Science* 74, E512–E518. <https://doi.org/10.1111/j.1750-3841.2009.01360.x>
- 445 Chiralt, A., Fito, P., 2003. Transport Mechanisms in Osmotic Dehydration: The Role of  
 446 the Structure: *Food Science and Technology International* 9, 179–186.  
 447 <https://doi.org/10.1177/1082013203034757>
- 448 Christiaens, S., Van Buggenhout, S., Houben, K., Jamsazzadeh Kermani, Z., Moelants,  
 449 K.R.N., Ngouémazong, E.D., Van Loey, A., Hendrickx, M.E.G., 2016. Process-  
 450 Structure-Function Relations of Pectin in Food. *Crit Rev Food Sci Nutr* 56, 1021–  
 451 1042. <https://doi.org/10.1080/10408398.2012.753029>
- 452 Ciampa, A., Dell’Abate, M.T., Masetti, O., Valentini, M., Sequi, P., 2010. Seasonal  
 453 chemical–physical changes of PGI Pachino cherry tomatoes detected by magnetic  
 454 resonance imaging (MRI). *Food Chemistry* 122, 1253–1260.  
 455 <https://doi.org/10.1016/j.foodchem.2010.03.078>
- 456 de Belie, N., Laustsen, A.M., Martens, M., Bro, R., Baerdemaeker, J.D., 2002. Use of  
 457 Physico-Chemical Methods for Assessment of Sensory Changes in Carrot Texture  
 458 and Sweetness During Cooking. *Journal of Texture Studies* 33, 367–388.  
 459 <https://doi.org/10.1111/j.1745-4603.2002.tb01354.x>
- 460 Edzes, H.T., van Dusschoten, D., Van As, H., 1998. Quantitative T2 imaging of plant  
 461 tissues by means of multi-echo MRI microscopy. *Magn Reson Imaging* 16, 185–  
 462 196. [https://doi.org/10.1016/S0730-725X\(97\)00274-9](https://doi.org/10.1016/S0730-725X(97)00274-9)
- 463 Gonzalez, M.E., Barrett, D.M., McCarthy, M.J., Vergeldt, F.J., Gerkema, E., Matser,  
 464 A.M., Van As, H., 2010. (1)H-NMR study of the impact of high pressure and  
 465 thermal processing on cell membrane integrity of onions. *Journal of food science*  
 466 75, E417–25. <https://doi.org/10.1111/j.1750-3841.2010.01766.x>
- 467 Goodman, B.A., Williamson, B., Simpson, E.J., Chudek, J.A., Hunter, G., Prior, D.A.M.,  
 468 1996. High field NMR microscopic imaging of cultivated strawberry fruit.  
 469 *Magnetic Resonance Imaging* 14, 187–196. [https://doi.org/10.1016/0730-725X\(95\)02051-T](https://doi.org/10.1016/0730-725X(95)02051-T)
- 470  
 471 Harker, F.R., Redgwell, R.J., Hallett, I.C., Murray, S.H., Carter, G., 1997. Texture of  
 472 Fresh Fruit, in: *Horticultural Reviews*. John Wiley & Sons, Ltd, pp. 121–224.  
 473 <https://doi.org/10.1002/9780470650646.ch2>

474 Hills, B.P., Duce, S.L., 1990. The influence of chemical and diffusive exchange on water  
475 proton transverse relaxation in plant tissues. *Magnetic Resonance Imaging* 8,  
476 321–331. [https://doi.org/10.1016/0730-725X\(90\)90106-C](https://doi.org/10.1016/0730-725X(90)90106-C)  
477 Hills, B.P., Remigereau, B., 1997. NMR studies of changes in subcellular water  
478 compartmentation in parenchyma apple tissue during drying and freezing.  
479 *International Journal of Food Science and Technology* 32, 51–61.  
480 <https://doi.org/10.1046/j.1365-2621.1997.00381.x>  
481 Istratov, A.A., Vyvenko, O.F., 1999. Exponential analysis in physical phenomena.  
482 *Review of Scientific Instruments* 70, 1233–1257.  
483 <https://doi.org/10.1063/1.1149581>  
484 Janssen, S., Verboven, P., Nugraha, B., Wang, Z., Boone, M., Josipovic, I., Nicolai, B.M.,  
485 2020. 3D pore structure analysis of intact ‘Braeburn’ apples using X-ray micro-  
486 CT. *Postharvest Biology and Technology* 159, 111014.  
487 <https://doi.org/10.1016/j.postharvbio.2019.111014>  
488 Kebe, M., Renard, C.M.C.G., El Maâtaoui, M., Amani, G.N.G., Maingonnat, J.-F., 2015.  
489 Leaching of polyphenols from apple parenchyma tissue as influenced by thermal  
490 treatments. *Journal of Food Engineering* 166, 237–246.  
491 <https://doi.org/10.1016/j.jfoodeng.2015.05.037>  
492 Khan, A.A., Vincent, J.F.V., 1990. Anisotropy of apple parenchyma. *Journal of the*  
493 *Science of Food and Agriculture* 52, 455–466.  
494 <https://doi.org/10.1002/jsfa.2740520404>  
495 Kim, D.M., Smith, N.L., Lee, C.Y., 1993. Apple Cultivar Variations in Response to Heat  
496 Treatment and Minimal Processing. *Journal of Food Science* 58, 1111–1114.  
497 <https://doi.org/10.1111/j.1365-2621.1993.tb06126.x>  
498 Kroeker, R.M., Henkelman, M.R., 1986. Analysis of biological NMR relaxation data with  
499 continuous distributions of relaxation times. *Journal of Magnetic Resonance*  
500 (1969) 69, 218–235. [https://doi.org/10.1016/0022-2364\(86\)90074-0](https://doi.org/10.1016/0022-2364(86)90074-0)  
501 Kunzek, H., Kabbert, R., Gloyna, D., 1999. Aspects of material science in food  
502 processing: changes in plant cell walls of fruits and vegetables. *Z Lebensm Unters*  
503 *Forsch* 208, 233–250. <https://doi.org/10.1007/s002170050410>  
504 Lahaye, M., Bouin, C., Barbacci, A., Le Gall, S., Foucat, L., 2018. Water and cell wall  
505 contributions to apple mechanical properties. *Food Chem* 268, 386–394.  
506 <https://doi.org/10.1016/j.foodchem.2018.06.110>  
507 Lawson, C.L., Hanson, R.J., 1995. Solving Least Squares Problems, *Classics in Applied*  
508 *Mathematics*. Society for Industrial and Applied Mathematics.  
509 <https://doi.org/10.1137/1.9781611971217>  
510 Le Bourvellec, C., Bouzerzour, K., Ginies, C., Regis, S., Plé, Y., Renard, C.M.G.C., 2011.  
511 Phenolic and polysaccharidic composition of applesauce is close to that of apple  
512 flesh. *Journal of Food Composition and Analysis*, 8th International Food Data  
513 Conference: Quality food composition data, key for health and trade 24, 537–547.  
514 <https://doi.org/10.1016/j.jfca.2010.12.012>  
515 Létal, J., Jiráček, D., Šuderlová, L., Hájek, M., 2003. MRI ‘texture’ analysis of MR images  
516 of apples during ripening and storage. *LWT - Food Science and Technology* 36,  
517 719–727. [https://doi.org/10.1016/S0023-6438\(03\)00099-9](https://doi.org/10.1016/S0023-6438(03)00099-9)  
518 Marigheto, N., Venturi, L., Hills, B., 2008. Two-dimensional NMR relaxation studies of  
519 apple quality. *Postharvest Biology and Technology* 48, 331–340.  
520 <https://doi.org/10.1016/j.postharvbio.2007.11.002>

- 521 McCarthy, M.J., Perez, E., Özilgen, M., 1991. Model for Transient Moisture Profiles of a  
522 Drying Apple Slab Using the Data Obtained with Magnetic Resonance Imaging.  
523 Biotechnology Progress 7, 540–543. <https://doi.org/10.1021/bp00012a009>
- 524 Mendoza, F., Verboven, P., Mebatsion, H.K., Kerckhofs, G., Wevers, M., Nicolai, B.,  
525 2007. Three-dimensional pore space quantification of apple tissue using X-ray  
526 computed microtomography. *Planta* 226, 559–570.  
527 <https://doi.org/10.1007/s00425-007-0504-4>
- 528 Mohoric, A., Vergeldt, F., Gerkema, E., van Dalen, G., van den Doel, L.R., van Vliet, L.J.,  
529 Van As, H., Van Duynhoven, J., 2009. The effect of rice kernel microstructure on  
530 cooking behaviour: A combined mu-CT and MRI study. *Food Chem.* 115, 1491–  
531 1499. <https://doi.org/10.1016/j.foodchem.2009.01.089>
- 532 Ng, A., Waldron, K.W., 1997. Effect of Cooking and Pre-Cooking on Cell-Wall Chemistry  
533 in Relation to Firmness of Carrot Tissues. *Journal of the Science of Food and*  
534 *Agriculture* 73, 503–512. [https://doi.org/10.1002/\(SICI\)1097-  
535 0010\(199704\)73:4<503::AID-JSFA762>3.0.CO;2-Z](https://doi.org/10.1002/(SICI)1097-0010(199704)73:4<503::AID-JSFA762>3.0.CO;2-Z)
- 536 Parada, J., Aguilera, J. m., 2007. Food Microstructure Affects the Bioavailability of  
537 Several Nutrients. *Journal of Food Science* 72, R21–R32.  
538 <https://doi.org/10.1111/j.1750-3841.2007.00274.x>
- 539 Ting, V.J.L., Silcock, P., Bremer, P.J., Biasioli, F., 2013. X-Ray Micro-Computer  
540 Tomographic Method to Visualize the Microstructure of Different Apple  
541 Cultivars. *Journal of Food Science* 78, E1735–E1742.  
542 <https://doi.org/10.1111/1750-3841.12290>
- 543 Valero, C., Ruiz-Altisent, M., Cubeddu, R., Pifferi, A., Taroni, P., Torricelli, A., Valentini,  
544 G., Johnson, D., Dover, C., 2004. Selection Models for the Internal Quality of  
545 Fruit, based on Time Domain Laser Reflectance Spectroscopy. *Biosystems*  
546 *Engineering* 88, 313–323. <https://doi.org/10.1016/j.biosystemseng.2004.03.012>
- 547 Van As, H., 2007. Intact plant MRI for the study of cell water relations, membrane  
548 permeability, cell-to-cell and long distance water transport. *J. Exp. Bot.* 58, 743–  
549 756. <https://doi.org/10.1093/jxb/erl157>
- 550 Van As, H., van Duynhoven, J., 2013. MRI of plants and foods. *J. Magn. Reson.* 229,  
551 25–34. <https://doi.org/10.1016/j.jmr.2012.12.019>
- 552 Van Buren, J.P., 1979. The Chemistry of Texture in Fruits and Vegetables. *Journal of*  
553 *Texture Studies* 10, 1–23. <https://doi.org/10.1111/j.1745-4603.1979.tb01305.x>
- 554 Waldron, K.W., Parker, M. l., Smith, A.C., 2003. Plant Cell Walls and Food Quality.  
555 *Comprehensive Reviews in Food Science and Food Safety* 2, 128–146.  
556 <https://doi.org/10.1111/j.1541-4337.2003.tb00019.x>
- 557 Whittall, K.P., MacKay, A.L., 1989. Quantitative interpretation of NMR relaxation data.  
558 *Journal of Magnetic Resonance* (1969) 84, 134–152.  
559 [https://doi.org/10.1016/0022-2364\(89\)90011-5](https://doi.org/10.1016/0022-2364(89)90011-5)
- 560 Winisdorffer, G., Musse, M., Quellec, S., Devaux, M.F., Lahaye, M., Mariette, F., 2015.  
561 MRI investigation of subcellular water compartmentalization and gas  
562 distribution in apples. *Magn. Reson. Imaging* 33, 671–680.  
563 <https://doi.org/10.1016/j.mri.2015.02.014>
- 564 Zerbini, P.E., Grassi, M., Cubeddu, R., Pifferi, A., Torricelli, A., 2002. Nondestructive  
565 detection of brown heart in pears by time-resolved reflectance spectroscopy.  
566 *Postharvest Biology and Technology* 25, 87–97. [https://doi.org/10.1016/S0925-  
567 5214\(01\)00150-8](https://doi.org/10.1016/S0925-5214(01)00150-8)

568 **Figures**

569

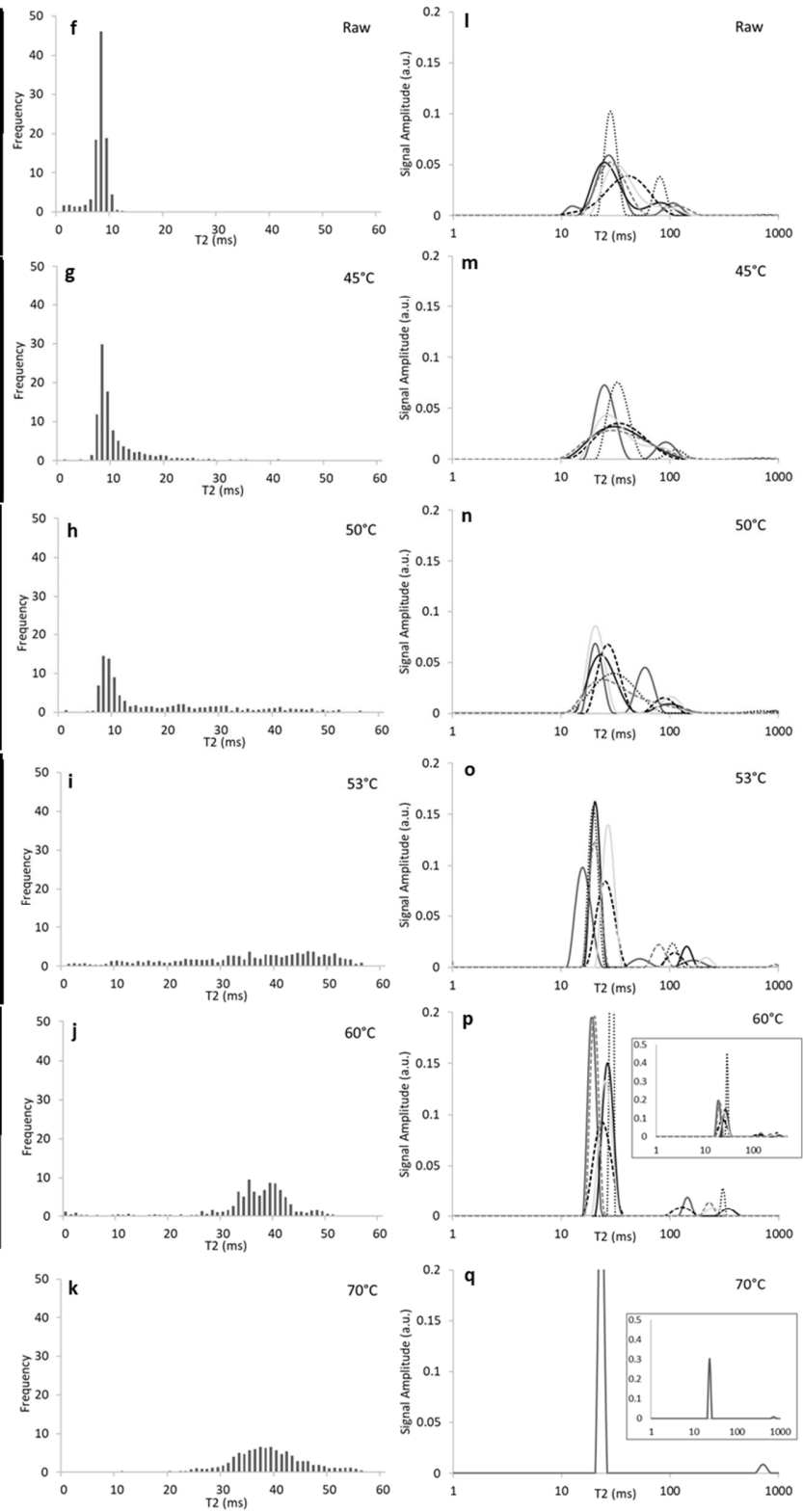
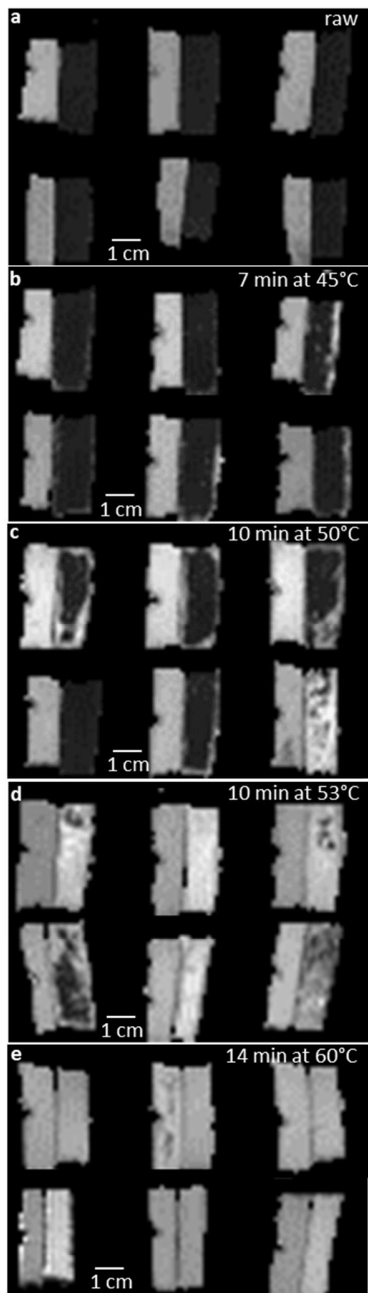


570

571 Figure 1: Mean Load ( $F_{\text{mean}}$ ) obtained by puncture tests on the apple sticks heated at the studied  
572 cooking temperatures (24 points per temperature, 20°C is the raw stick)

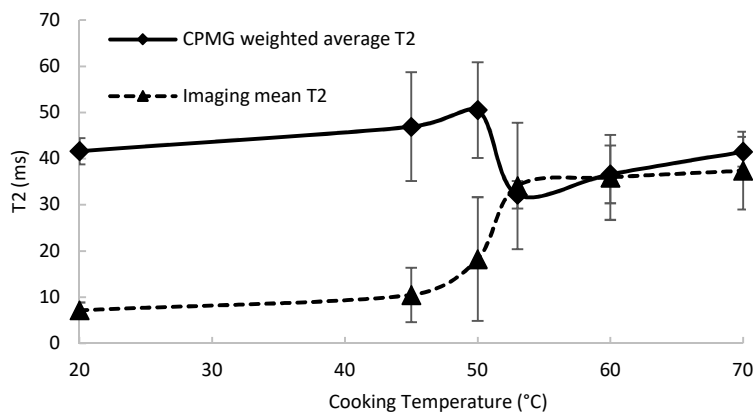
573





575 Figure 2:  $T_2$  maps windowed from 0 to 60 ms (left) for raw (a), 45 °C (b), 50 °C (c), 53 °C (d) and  
 576 60 °C (e) thermal treatment. The six samples are displayed for each thermal treatment. For each  
 577 sample, the treated sample (on the right) is placed against a reference sample (on the left)  
 578 cooked for 18 min at 70 °C. Distribution of  $T_2$  within the samples (middle) for raw (f), 45 °C (g),  
 579 50 °C (h), 53 °C (i), 60 °C (j) and 70 °C (k).  $T_2$  distribution, obtained with CPMG, for the 6  
 580 samples at raw (l), 45 (m), 50 (n), 53 (o), 60 (p) and 70 °C (q).

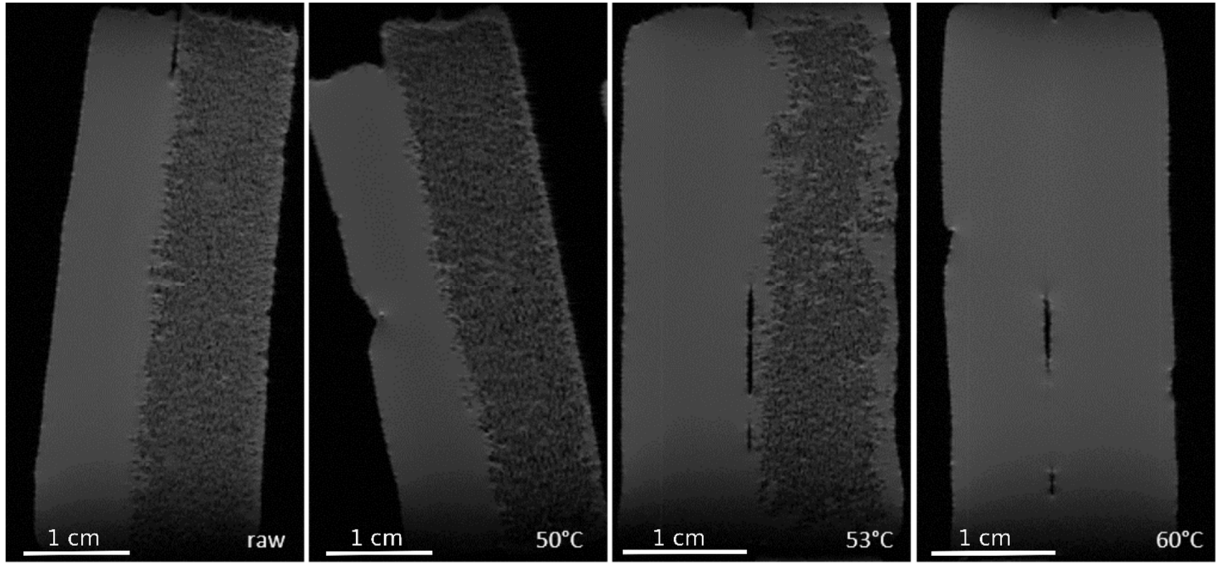
581  
 582



583

584 Figure 3:  $T_2$  variation with cooking temperature. 20°C means raw sample. Solid line: PMG  
 585 average  $T_2$ . This average is weighted by the population of each  $T_2$  value. Dotted line: imaging  $T_2$   
 586 averaged over the whole images of samples cooked at a given cooking temperature.

587  
 588



589

590 Figure 4: High-resolution MRI images of raw, and 50, 53 and 60 °C treated samples. The left  
591 sticks are the reference cooked (70 °C) samples.

592

593

594

595